# Ultra-high order ring resonator system with sharp transmission peaks

**S. H. Tao[*,1], S. C. Mao[1,2], J. F. Song[1,3], Q. Fang[1], M. B. Yu[1], G. Q. Lo[1], and D. L. Kwong[1]**

**School of Physical Science and Technology, Central South University, 410083, China*
*[1]Institute of Microelectronics, A*STAR, 11 Science Park Road, Science Park II, Singapore 117685*
[2]School of Electrical and Information Engineering, Xi'an Jiaotong University, 710049, China
*[3]State Key Laboratory on Integrated Opto-Electronics, College of Electronic Science and Engineering, Jilin University, 130023, China*

**Abstract:** We propose a relay ring resonator structure which comprises multiple cascaded microring resonators, in which the drop waveguide of a microring resonator is also the input waveguide of the subsequent microring resonator, and so forth. Thus, the transmission response of the relay ring resonator structure has sharp peaks, high out-of-band rejection ratios, and long group delays. A relay ring resonator structure comprising 90 microrings is fabricated on silicon nitride wire waveguides. The simulation and experimental results are in good agreement.



**OCIS codes:** (230.5750) Resonators; (130.3120) Integrated optical devices; (220.0220) Optical design and fabrication.

## References and links

1. S. Xiao, M. H. Khan, H. Shen, and M. Qi, "Multiple-channel silicon micro-resonator based filters for WDM applications," Opt. Express **15**(12), 7489–7498 (2007), http://www.opticsinfobase.org/abstract.cfm?URI=oe-15-12-7489.
2. G. Lenz, and C. K. Madsen, "General optical all-pass filter structures for dispersion control in WDM systems," J. Lightwave Technol. **17**(7), 1248–1254 (1999).
3. C. Y. Chao, W. Fung, and L. J. Guo, "Polymer microring resonators for biochemical sensing applications," IEEE J. Sel. Top. Quantum Electron. **12**(1), 134–142 (2006).
4. C. K. Madsen, and G. Lenz, "Optical all-pass filters for phase response design with applications for dispersion compensation," IEEE Photon. Technol. Lett. **10**(7), 994–996 (1998).
5. G. Lenz, B. J. Eggleton, C. K. Madsen, and R. E. Slusher, "Optical delay lines based on optical filters," IEEE J. Quantum Electron. **37**(4), 525–532 (2001).
6. V. R. Almeida, and M. Lipson, "Optical bistability on a silicon chip," Opt. Lett. **29**(20), 2387–2389 (2004).
7. A. C. Turner, M. A. Foster, A. L. Gaeta, and M. Lipson, "Ultra-low power parametric frequency conversion in a silicon microring resonator," Opt. Express **16**(7), 4881–4887 (2008), http://www.opticsinfobase.org/abstract.cfm?URI=oe-16-7-4881.
8. S. Y. Cho, and R. Soref, "Interferometric microring-resonant 2 x 2 optical switches," Opt. Express **16**(17), 13304–13314 (2008), http://www.opticsinfobase.org/abstract.cfm?URI=oe-16-17-13304.
9. F. Xia, L. Sekaric, and Y. Vlasov, "Ultracompact optical buffers on a silicon chip," Nat. Photonics **1**(1), 65–71 (2007).
10. B. E. Little, S. T. Chu, P. P. Absil, J. V. Hryniewicz, F. G. Johnson, F. Seiferth, D. Gill, V. Van, O. King, and M. Trakalo, "Very high-order microring resonator filters for WDM applications," IEEE Photon. Technol. Lett. **16**(10), 2263–2265 (2004).
11. M. A. Popovíc, T. Barwicz, M. R. Watts, P. T. Rakich, L. Socci, E. P. Ippen, F. X. Kärtner, and H. I. Smith, "Multistage high-order microring-resonator add-drop filters," Opt. Lett. **31**(17), 2571–2573 (2006).
12. S. C. Mao, S. H. Tao, Y. L. Xu, X. W. Sun, M. B. Yu, G. Q. Lo, and D. L. Kwong, "Low propagation loss SiN optical waveguide prepared by optimal low-hydrogen module," Opt. Express **16**(25), 20809–20816 (2008), http://www.opticsinfobase.org/oe/abstract.cfm?URI=oe-16-25-20809.
13. J. K. S. Poon, J. Scheuer, S. Mookherjea, G. T. Paloczi, Y. Huang, and A. Yariv, "Matrix analysis of microring coupled-resonator optical waveguides," Opt. Express **12**(1), 90–103 (2004), http://www.opticsinfobase.org/abstract.cfm?URI=oe-12-1-90.
14. R. Grover, V. Van, T. A. Ibrahim, P. P. Absil, L. C. Calhoun, F. G. Johnson, J. V. Hryniewicz, and P.-T. Ho, "Parallel-cascaded semiconductor microring resonators for high-order and wide-FSR filters," J. Lightwave Technol. **20**(5), 900–905 (2002).
15. G. Griffel, "Vernier Effect in Asymmetrical Ring Resonator Arrays," IEEE Photon. Technol. Lett. **12**(12), 1642–1644 (2000).
16. B. E. Little, S. T. Chu, W. Pan, and Y. Kokubun, "Microring resonator arrays for VLSI photonics," IEEE Photon. Technol. Lett. **12**(3), 323–325 (2000).

#113900 - $15.00 USD Received 8 Jul 2009; revised 11 Sep 2009; accepted 24 Sep 2009; published 4 Jan 2010

17. F. J. Fraile-Peláez, and P. Chamorro-Posada, "Active control and stability in microring resonator chains," Opt. Express **15**(6), 3177–3189 (2007), http://www.opticsinfobase.org/abstract.cfm?URI=oe-15-6-3177.
18. J. Capmany, P. Muñoz, J. D. Domenech, and M. A. Muriel, "Apodized coupled resonator waveguides," Opt. Express **15**(16), 10196–10206 (2007), http://www.opticsinfobase.org/abstract.cfm?URI=oe-15-16-10196.

## 1. Introduction

Microring resonators can be widely used as optical filters [1, 2], optical sensors [3], dispersion compensators [4, 5], modulators [6], wavelength converters [7], optical switches [8], optical buffers [9], and so on. For instances, based on the transmission response characteristics, photonic wire ring resonators with flat passbands and high out-of-band rejection ratio (ORR) can be used as add/drop wavelength filters for DWDM (Dense Wavelength Division Multiplexing) applications in optical communications while microring resonators with high Q factors are sensitive to the wavelength shift and can be used as high-precision sensors to detect ultra-low sample concentrations. In recent years, high order ring resonators have been receiving increasing interests owing to the fast development of complementary metal-oxide semiconductor (CMOS) fabrication technology for micro- and nano-photonic devices and promising applications of high-density photonic integrated circuits [9,10]. Microring resonators can be fabricated with CMOS-compatible process technology with high throughput, low cost, and monolithic integration. Silicon nitride (SiN) is a candidate for the waveguide material of ring resonator structures [11] as it has high refractive index (2.0~2.4) and low absorption loss at the communications bands and can be conveniently deposited with LPCVD (Low Pressure Chemical Vapor Deposition) or PECVD (Plasma Enhanced Chemical Vapor Deposition). The propagation loss of a single-mode SiN waveguide can be as low as ~2.1 dB/cm [12].

To achieve high performance of transmission responses, researchers widely adopt higher order (number of rings N>1) and ultra-high order (N>10) microring resonators. Many kinds of coupled ring resonators have been reported, such as serial-cascaded coupled resonator optical waveguides (CROW) [13], parallel-cascaded ring resonators [14, 15], and mix-coupled ring resonators [16]. High order CROW resonators normally have flat passbands, sharp rolloffs, high ORRs, and long group delays. There is a tradeoff between the transmittance and the delay, i.e., the longest delay appears at the lowest transmittance of the device, and vice versa. The parallel-cascaded ring resonators also have flat passbands and sharp rolloffs [14]. The free spectral range (FSR) can be expanded due to Vernier effect [14, 15]. However, the powers of the suppressed resonance modes are still rather high compared with those of the desired ones [14]. The mix-coupled ring resonators such as arrays of coupled rings can achieve customized transmission responses. However, a large number of interconnect paths and recirculating loops could lead to complicated transmission responses [16].

In this letter we propose a relay ring resonator structure which comprises many microrings. The drop waveguide of the first microring is the input waveguide of the second ring, and so forth. With such an arrangement, each ring resonator in the cascades will filter the input light and relay the filtered light to the next cascade. Thus, the transmission of the relay ring resonator structure will have sharper rolloffs, higher ORRs, and longer group delays. In addition, compared with the CROW structures, the relay ring resonator structures have sharpened transmission peaks instead of flattened peaks at the drop ports. Although a single ring resonator can achieve sharp transmissions with controlled fabrication process, the delay is still too short for optical buffering or dispersion compensation. Moreover, the transmission ORR of a single ring seldom exceeds 20 dB whereas high ORR is vital for the components in commercial applications. For the ultra-high order ring resonator system, its sharp transmissions and many available ports could be useful in sensor and group delay applications. As transmission peaks become sharper with the increase of the number of the rings, we can obtain customized bandwidths of the transmissions from one of the cascades of the ultra-high order ring resonator system. In addition, as light can be coupled out from each cascade of the ring resonator system, many cascades in the ultra-high order ring resonator system can be used simultaneously for analysis of multiple samples. As group delay at each

#113900 - $15.00 USD Received 8 Jul 2009; revised 11 Sep 2009; accepted 24 Sep 2009; published 4 Jan 2010

cascade is different and increases with the number of the cascades, we can find transmissions with the desired group delay from a cascade of such an ultra-high order ring resonator system. In this work, in addition to design and theoretic analysis, an ultra-high order ring resonator system with 90 relay rings fabricated on SiN core layer enclosed with silicon dioxide will be experimentally demonstrated.

## 2. Design and analysis

The layout of a schematic relay ring resonator structure is shown in Fig. 1. The proposed relay ring resonator structure comprises many rings and coupling waveguides. Each ring resonator is coupled with an input/through and an add/drop waveguides. The drop waveguide of the first ring is also used as the input waveguide of the second ring; similarly, the drop waveguide of the second ring is also the input waveguide of the third ring, and so on. Light in the drop port of the first ring would be filtered again by the second ring, and the filtered drop light in the second ring would be relayed to the third ring, and so forth. Thus, the peaks of the transmission spectrum would become sharper and sharper. At the same time, the ORR would be greatly improved.

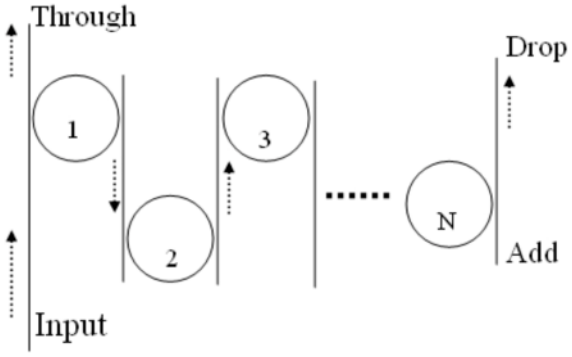


Fig. 1. Layout of the relay ring resonator structure. The dashed arrows represent the propagation directions of light.

In Fig. 1, the dashed arrows stand for the directions of light propagations. All the rings and waveguides are identical with the same radius or cross-section, and the gap widths of all the coupling gaps are also the same. We can collect the drop light of any ring by extending the corresponding drop waveguide to a power receiver. Note that only the light at resonance wavelengths can pass through the cascades of the rings. Although the drop waveguide of a ring also contains the through transmission light of the next ring, the through light would be negligible if the cross-coupling coefficient approaches to 1. Based on the transfer matrix theory [13], we can deduce the transmissions at the through port of the first ring and the drop ports of the subsequent rings. For the first ring, the inputs and outputs can be described by,

$$\begin{bmatrix} a_{add}^{(1)} \\ b_{drop}^{(1)} \end{bmatrix} = PQP \begin{bmatrix} a_{input}^{(1)} \\ b_{through}^{(1)} \end{bmatrix} \tag{1}$$

$$P = \frac{1}{\kappa}\begin{bmatrix} -t & 1 \\ -1 & t^* \end{bmatrix} \tag{2}$$

$$Q = \begin{bmatrix} 0 & \exp(-i\beta R\pi) \\ \exp(i\beta R\pi & 0 \end{bmatrix} \tag{3}$$

$$PQP = \begin{bmatrix} A & B \\ C & D \end{bmatrix} \tag{4}$$

#113900 - $15.00 USD Received 8 Jul 2009; revised 11 Sep 2009; accepted 24 Sep 2009; published 4 Jan 2010

where, $a_{input}^{(1)}$, $a_{add}^{(1)}$ stand for the complex amplitudes of lights at the input and add ports of the first resonator, $b_{through}^{(1)}$, $b_{drop}^{(1)}$ stand for the complex amplitudes of lights at the through and drop ports of the first resonator, respectively. $\kappa$ and $t$ are cross- and self-coupling coefficients, respectively, and $|\kappa|^2 + |t|^2 = 1$ stands for a lossless coupling. $R$ is the radius of the ring. $\beta$ is the propagation constant and $\beta = n(\lambda)2\pi / \lambda + i\alpha$, where $n(\lambda)$ is the effective index at wavelength $\lambda$, and $\alpha$ is amplitude attenuation factor.

Assume $a_{add}^{(1)} = 0$ and we can obtain the transmissions at both the through and the drop ports of the first ring,

$$b_{through}^{(1)} = -\frac{A}{B} a_{input}^{(1)} \tag{5}$$

$$b_{drop}^{(1)} = (C - \frac{AD}{B}) a_{input}^{(1)} \tag{6}$$

Light at the drop port of the first ring will propagate a distance of $L$ along the straight drop waveguide and is coupled to the second ring. In this case, light in the input port of the second ring can be expressed by,

$$a_{input}^{(2)} = b_{drop}^{(1)} \cdot \exp(-i\beta L) \tag{7}$$

Similarly, light in the drop port of the second ring will be deduced from Eqs. (1-6). And light at the drop port of the nth ring can be written by,

$$a_{input}^{(n)} = b_{drop}^{(n-1)} \cdot \exp(-i\beta L) \tag{8}$$

$$b_{drop}^{(n)} = (C - \frac{AD}{B}) a_{input}^{(n)} \tag{9}$$

The group delay of a single ring can be determined using the following expression [17,18],

$$\tau = -\frac{1}{c} \frac{d\phi(k)}{dk} \tag{10}$$

where $c$ is the light velocity in vacuum, $\varphi(k)$ is the phase of the output light, and $k = 2\pi / \lambda$. Thus, based on the complex amplitudes of the transmission spectrum of the nth ring, we can infer the delay response using Eq. (10). It is worth mentioning that the obtained phase values from Eq. (10) should be unwrapped before differentiated.

### 3. Device fabrication and characterization

We started the fabrication on a 200 mm crystalline silicon wafer. First, we deposited 5 μm silicon dioxide with PECVD as the insulating layer. Then, we polished the surface of the deposited silicon dioxide layer with a typical Oxide CMP (Chemical-Mechanical Polishing) process, so the surface roughness of the oxide layer will not affect the subsequent PECVD deposition of the SiN layer, and the scattering loss of light will be also reduced. 400 nm SiN was deposited with PECVD as waveguide core layer. The refractive index of the SiN film was ~2.06. Then we coated the SiN layer with photo-resist, followed by 248 nm deep-UV lithography. We etched the patterned SiN layer with inductively coupled plasma, stripped off the unexposed photo-resist, and cleaned the wafer with diluted HF and sulfuric acid-hydrogen peroxide mixture solutions. Finally, we clad the wafer uniformly with 3 μm high density plasma (HDP) oxide with PECVD. Three scanning electron microscope (SEM) pictures for a fabricated waveguide, a coupling region between a waveguide and a ring, and an inverse taper

#113900 - $15.00 USD Received 8 Jul 2009; revised 11 Sep 2009; accepted 24 Sep 2009; published 4 Jan 2010

are present in Figs. 2(a), (b), and (c), respectively. The inverse taper is used for efficient light coupling between a sub-micron waveguide and a lensed single-mode fiber. Note that the SEM pictures of the displaying components were taken before the top silicon dioxide cladding was deposited. An optical microscope picture of part of the structure is shown in Fig. 2(d), where two rows of relay rings are displayed and the longest straight waveguide in the left is the input/through waveguide of the first ring. The rings are arranged in multiple rows, so the width of the whole structure can be reduced. In the fabricated structure the through waveguide of the first ring and the drop waveguides of the 32nd ring, 62nd ring, and 90th ring had been chosen for optical measurement.

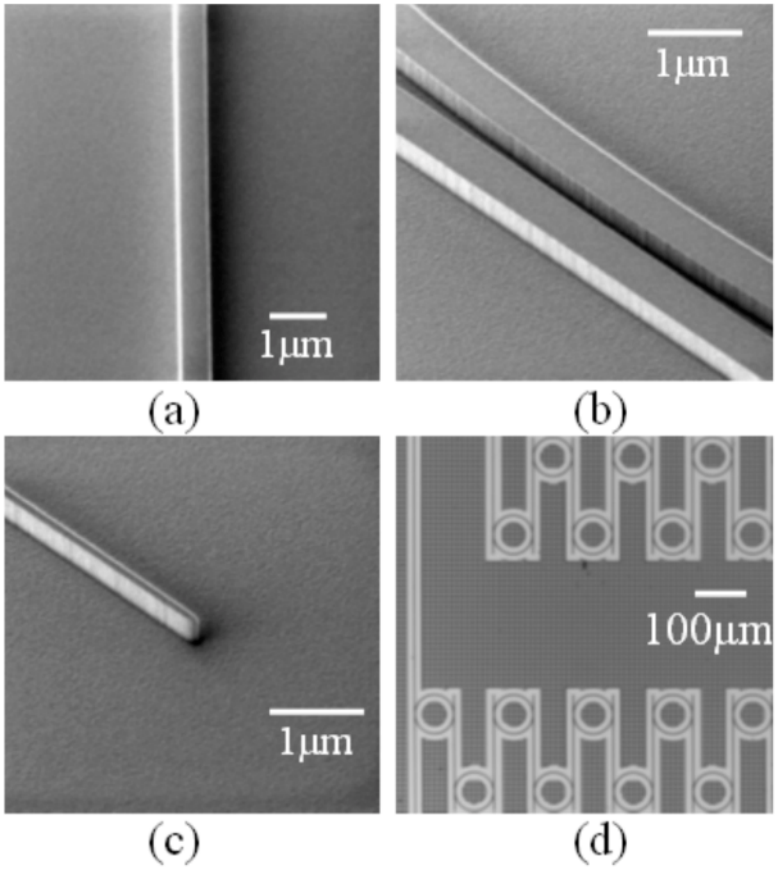


Fig. 2. SEM pictures of (a) a SiN wire waveguide, (b) a coupling region of a straight waveguide and a ring, and (c) an inverse taper. (d) Optical microscope picture of part of the fabricated 90 relay ring resonator structure. The rings are arranged in multiple rows to decrease the width of the full device, and the longest waveguide in the utmost left is the input/through waveguide of the first ring.

The structural parameters of the fabricated structure are as follows. The cross-section of the waveguides is 700 nm × 400 nm, the coupling gap width is 250 nm, the radius of the rings is 40 μm, and the length of the straight coupling waveguides between two neighboring rings is 160 μm. The inverse taper is 200 μm long with a tip width of 180 nm. There are totally 90 rings in the device and the full length of the device is 3 mm. The 90 rings cover a total area of ~2600 μm × 700 μm.

We diced the wafer into many sample pieces and manually polished the coupling facets of the samples with diamond films for better light coupling between the inverse taper and a lensed single-mode fiber. In the characterization, we connected the tunable laser and the power meter of an optical spectrum analyzer system (EXFO IQS-12004B) with a

#113900 - $15.00 USD Received 8 Jul 2009; revised 11 Sep 2009; accepted 24 Sep 2009; published 4 Jan 2010

polarization-maintaining single-mode fiber. The wavelength was scanned from 1510 nm to 1612 nm with step of 5 pm and the corresponding readings in the power meter were recorded as the reference insertion losses. Two lensed polarization maintaining fibers (LPMFs) for coupling input and output lights were mounted on two high-precision three-dimensional stages, respectively. The focus spot of the LPMF was ~2.5 μm in diameter. Then, we placed a device on a sample stage and aligned both the input and output coupling facets of the device with the mounted LPMFs, respectively. Finally, TE (Transverse Electric) mode insertion losses of the device were measured with the same scanning range and resolution. The insertion losses included the fiber-waveguide coupling losses and transmission losses of the device. The measured transmission spectrum at the drop port of the 90th ring is shown in Fig. 3. It can be observed that the absolute value of ORR exceeds 40 dB in the range of 1540 nm ~1612 nm. The ORR could be even higher if sufficient sensitivity of the power meter is available to reveal. The splits observed in the resonance peaks are caused by slight dimension mismatches of the rings, gaps, and waveguides due to fabrication variations. The measured FSR around the wavelength of 1550 nm is ~5 nm.

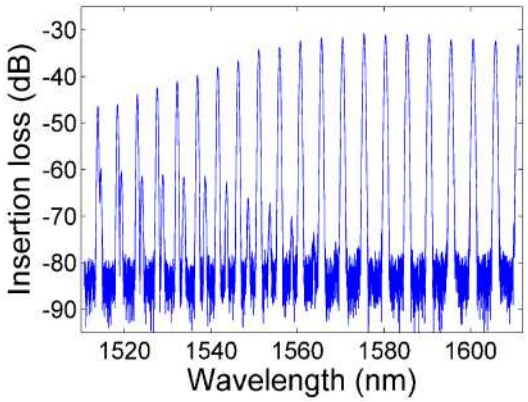


Fig. 3. Transmission spectrum at the drop port of the 90th ring.

We also measured spectra at the drop ports of the 32nd and 62nd rings, respectively. For comparison, the normalized spectra of the 32nd, 62nd, and 90th rings at wavelength ~1551 nm are present in Fig. 4. It can be seen that the 90th ring has the sharpest peak. This effect is contrary to those of the serial-coupled CROW structures, which flatten the spectra instead. It was found that the 90th ring also had the highest ORR. A dip can be seen in both the transmission peaks of the 32nd and 62nd rings. The dips could be caused by the partial power transfer from the drop waveguides of the rings to the inputs of the subsequent cascade rings, as both the drop waveguides of the 32nd ring and the 62nd ring are also the input waveguides of the subsequent rings. There is no such a dip in the drop transmission of the 90th ring as the drop waveguide solely outputs the light and does not transfer light to any subsequent cascade.

#113900 - $15.00 USD Received 8 Jul 2009; revised 11 Sep 2009; accepted 24 Sep 2009; published 4 Jan 2010

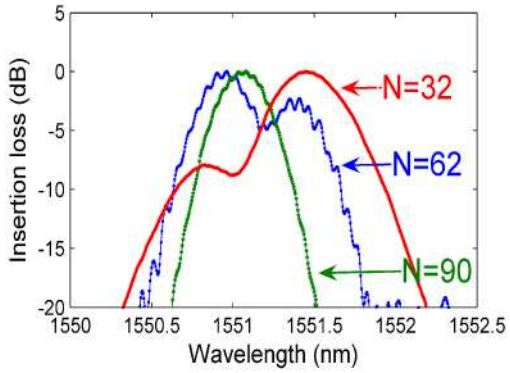


Fig. 4. Normalized transmission peaks at ~1551 nm at the drop ports of the 32nd, 62nd, and 90th rings, respectively.

To characterize the performance of the SiN wire waveguides, we also fabricated a series of paper-clip like SiN waveguides with the same structural parameters and varying waveguide lengths on the same wafer. The propagation loss of the SiN wire waveguides was measured as ~2.5 dB/cm at 1550 nm with the cutback method. The on-chip loss for the 90-ring spectral responses is ~-20 dB at 1550 nm. There are four factors affecting the on-chip loss of the relay ring resonator structure: the self- and cross- coupling coefficients, the amplitude attenuation factor, and the number of rings. We can deduce the coupling coefficients and the average amplitude attenuation factor by fitting the experimental spectra with simulated spectra, which are obtained based on Eqs. (1-9). The experimental through transmission in the first ring and the experimental drop transmission in the last ring, i.e. the 90th ring, at ~1550 nm, are shown as solid lines in Fig. 5. The fitting transmissions with the same structural parameters as those of the measured are also shown as dashed lines in Fig. 5. The fitting coupling coefficients $\kappa$ and $t$ are 0.80312 and 0.59582, respectively. The average amplitude attenuation factor is 3.47 dB/cm, which is higher than the waveguide propagation loss obtained from the previous cutback measurement as the amplitude attenuation factor includes both the waveguide propagation loss and the through transmission loss in the waveguide-ring coupling. The ultra-high order ring resonator system is polarization dependent. The polarization sensitivity of the ring resonator structure mainly depends on the waveguide structure, the couplings, and the arrangements of the ring resonators. To reduce the polarization sensitivity, we need re-design the waveguide structure, for example, to use a waveguide with near-square cross-section. In Fig. 5, the dip in the experimental through transmission is not as deep as that in the simulation. Two factors might cause the difference: in the experiment we used LPMFs to couple light and the polarization orientation was controlled by a polarization controller. However, the polarization orientation of the input light might not be aligned exactly with that of the device. And in the simulations we used average coupling coefficients to calculate the transmissions of all the couplings. The average coupling coefficients may not fit the specified coupling between the through waveguide and the first ring.

#113900 - $15.00 USD Received 8 Jul 2009; revised 11 Sep 2009; accepted 24 Sep 2009; published 4 Jan 2010

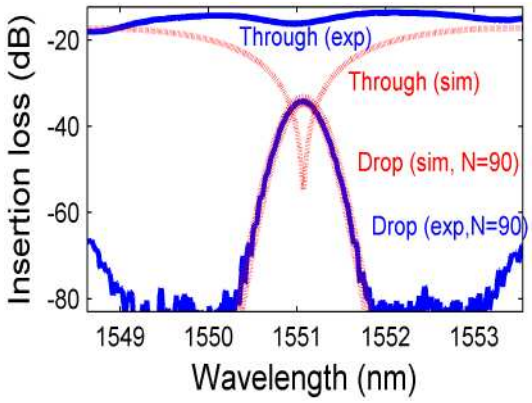


Fig. 5. Curves from top to bottom are: experimental through transmission (solid line) and simulated through transmission (dashed line) of the first ring, and the simulated drop transmission (dashed line) and experimental drop transmission (solid line) of the 90th ring.

Since we have obtained the coupling coefficients for the 90-relay-ring resonator structure by fitting the experimental drop spectrum, the group delay can be calculated based on Eq. (10). The group delay is found to exceed 150 ps.

We have fabricated many such devices in different wafers and batches, and found the performances of such devices are consistent. This means that the fabrication of such devices is repeatable and does not need special process control. In the proposed structure, as the preceding cascades control the inputs of the subsequent cascades, misalignment and size variation of the components in the preceding rings would result in frequency shift of the transmissions of the subsequent rings. However, misalignment and size variation of the components in the subsequent cascades will have negligible influences on the transmissions of the preceding cascades.

## 4. Conclusion

In summary, we have demonstrated a relay ring resonator structure comprising 90 identical microrings fabricated on SiN wire waveguides. The drop light in a ring resonator is the input light of the next ring resonator and so forth. With such an arrangement, higher order relay microring resonator structure have higher ORRs, sharper peaks, and longer group delays in the transmission responses while the FSR remains roughly the same as that of a single ring with the same radius. There are many ports in the system and light can be lost from the idling ports, so the measured losses were quite high for the higher cascades. Amplification can be used to boost the signal strength of the higher cascades. The relay ring resonator structure could find many applications as optical filters, optical sensors, optical buffers, and so on.

#113900 - $15.00 USD Received 8 Jul 2009; revised 11 Sep 2009; accepted 24 Sep 2009; published 4 Jan 2010